

SAM-IQA: Can Segment Anything Boost Image Quality Assessment ?

Xinpeng Li^{1*} Ting Jiang^{1*} Haoqiang Fan¹ Shuaicheng Liu^{2,1†}
¹ Megvii Technology
² University of Electronic Science and Technology of China

Abstract

Image Quality Assessment (IQA) is a challenging task that requires training on massive datasets to achieve accurate predictions. However, due to the lack of IQA data, deep learning-based IQA methods typically rely on pre-trained networks trained on massive datasets as feature extractors to enhance their generalization ability, such as the ResNet network trained on ImageNet. In this paper, we utilize the encoder of Segment Anything, a recently proposed segmentation model trained on a massive dataset, for high-level semantic feature extraction. Most IQA methods are limited to extracting spatial-domain features, while frequency-domain features have been shown to better represent noise and blur. Therefore, we leverage both spatial-domain and frequency-domain features by applying Fourier and standard convolutions on the extracted features, respectively. Extensive experiments are conducted to demonstrate the effectiveness of all the proposed components, and results show that our approach outperforms the state-of-the-art (SOTA) in four representative datasets, both qualitatively and quantitatively. Our experiments confirm the powerful feature extraction capabilities of Segment Anything and highlight the value of combining spatial-domain and frequency-domain features in IQA tasks. Our codes are available at <https://github.com/Hedlen/SAM-IQA>.

1. Introduction

Image Quality Assessment (IQA) plays a crucial role in image processing by providing an objective evaluation of image quality based on human preferences. Accurate IQA is beneficial for various image-related tasks, including Super Resolution (SR) [1–5], Image Denoising [6–8], and High Dynamic Range (HDR) imaging [9–11]. IQA approaches can be broadly classified into two categories: reference-based and reference-free methods. Reference-based methods require a reference image as a comparison during the evaluation process. These methods measure the

perceptual difference between the distorted image and the reference image to assess the quality. On the other hand, reference-free methods do not rely on a reference image and instead directly estimate the quality score based on the distorted image’s features. Reference-free methods are particularly useful when a reference image is not available or practical to obtain.

IQA is a subjective evaluation process that incorporates human experience to assess image quality. However, to enable models to perform IQA, they require extensive training on large datasets. Existing IQA datasets often lack sufficient information to support accurate model judgments. Consequently, current methods rely on pre-trained models for feature extraction as a reference for evaluation. For instance, ResNet [12], pre-trained on ImageNet, is widely used in various IQA approaches and consistently delivers outstanding performance.

Recently, there has been a trend toward using models trained on massive datasets to improve performance. The well-known large language models (LLMs) [13–15] have achieved revolutionary advancements in their field. Similarly, the recently proposed Segment Anything (SAM) [16] is a semantic segmentation model trained on an extensive dataset. With its abundant training samples and exceptional generalization ability, SAM attains state-of-the-art performance in comprehensive object segmentation. Its powerful segmentation and feature extraction capabilities have found wide application across various domains. In this paper, we introduce SAM as a feature extraction encoder in IQA. By leveraging SAM’s robust training and feature extraction capabilities, we aim to enhance IQA performance. This approach allows us to leverage the strengths of SAM and exploit its potential for accurate and efficient image quality assessment.

Existing IQA methods can be categorized into spatial-domain-based and frequency-domain-based approaches, depending on the type of features utilized. While most current methods rely on spatial-domain features, it has been demonstrated that frequency-domain features can better represent various image distortions such as noise and blur. Traditional frequency-domain-based methods often

*Equal contribution

†Corresponding author

employed strategies like Discrete Cosine Transform (DCT). However, with the advancements in deep learning, there has been a surge in deep learning-based methods for extracting frequency-domain features. Among these methods, Fourier convolution stands out as a prominent approach [17]. Fourier convolution involves applying Fourier transforms within neural networks. According to the spectral convolution theorem, modifying a value in the frequency domain would have a global impact on the original signal. By incorporating Fourier convolution, we can achieve a broader receptive field that captures information from the entire image, in contrast to spatial-domain convolutions that focus on local regions. This allows us to capture global features and relationships between different components of the image, which can further improve the accuracy of IQA method.

To sum up, our main contributions include:

- We are the first to introduce the SAM encoder as a feature extractor in IQA and demonstrate its strong generalization ability in this domain.
- We propose a method that integrates information from both frequency-domain and spatial-domain features.
- We conducted extensive experiments on commonly used benchmarks and showed that our approach outperforms state-of-the-art methods.

2. Related Work

2.1. Image Quality Assessment

Image Quality Assessment (IQA) aims to simulate human evaluation of image quality. Traditional IQA methods can be classified into three types based on the presence or absence of a reference image and the type of reference image used: Full-Reference IQA (FR-IQA), Reduced-Reference IQA (RR-IQA), and No-Reference IQA (NR-IQA).

FR-IQA is currently the most accurate and widely used form of image quality assessment. PSNR and SSIM [18] are two well-known FR-IQA methods that are commonly employed in various image-based tasks, including HDR imaging [9] and SR [4]. Traditional FR-IQA methods typically measure the differences between low-quality (LQ) and high-quality (HQ) images by comparing pixels or utilizing hand-designed features. In recent years, deep learning-based approaches have made significant advancements in FR-IQA. These methods utilize neural networks to extract image features, and some employ Neural Network (NN)-based models like transformers to perform the IQA task [19]. In a recent study by Cao et al. [20], a semi-supervised approach was employed, leveraging unlabeled data to make predictions. However, FR-IQA has strict re-

quirements for reference images, which limits its applicability in many scenarios. To address this limitation, researchers have proposed RR-IQA and NR-IQA methods. For instance, Zheng et al. [21] introduced an RR-IQA method where they first restore the LQ image and then utilize the restored image as the reference for comparison. The advancements in FR-IQA, including the application of deep learning-based methods and the development of RR-IQA and NR-IQA approaches, have significantly improved image quality assessment, enabling more versatile usage across a wide range of applications.

NR-IQA, in contrast, has wider application prospects, because it does not require any references during the assessment. [22] adopts the Convolution Neural Network (CNN) to the NR-IQA for the first time. Since then, many NN-based methods have been proposed [23,24]. [23] did not regress the mean opinion scores (MOS), but the quality map reduced the difficulty of the regression. Some prior knowledge is also incorporated during the evaluation [24,25]. However, as pointed out by [26], humans are good at comparing two images instead of looking at only one image. Therefore, no reference approaches are often less accurate than reference approaches.

2.2. Segment Anything.

Large-scale foundation models have achieved remarkable success in both natural language processing (NLP) and computer vision (CV) domains. These models are typically pre-trained on extensive datasets using specific tasks, enabling efficient fine-tuning and knowledge transfer to downstream tasks. Segment Anything (SAM) is a notable large-scale foundation model in semantic segmentation. By learning from 1 billion masks on 11 million images with 636 million parameters (ViT-H). SAM can segment all potential objects in an image without being affected by the image quality. This unique property allows us to design a novel SAM-guided refinement module that effectively enhances existing methods in various applications.

SAM has been widely adopted across different research fields, demonstrating its effectiveness and generalization capabilities. For example, Lu et al. [27] have successfully applied SAM in video super-resolution tasks to segment objects in the scene and mitigate the impact of large motions. In medical imaging, Ma et al. [28] have achieved excellent segmentation results by leveraging SAM. Furthermore, SAM has been utilized by Yu et al. [29] for inpainting arbitrary objects, showcasing its versatility beyond traditional segmentation tasks.

The broad adoption of SAM and its remarkable performance across diverse applications highlight its utility and effectiveness as a powerful tool in various research domains.

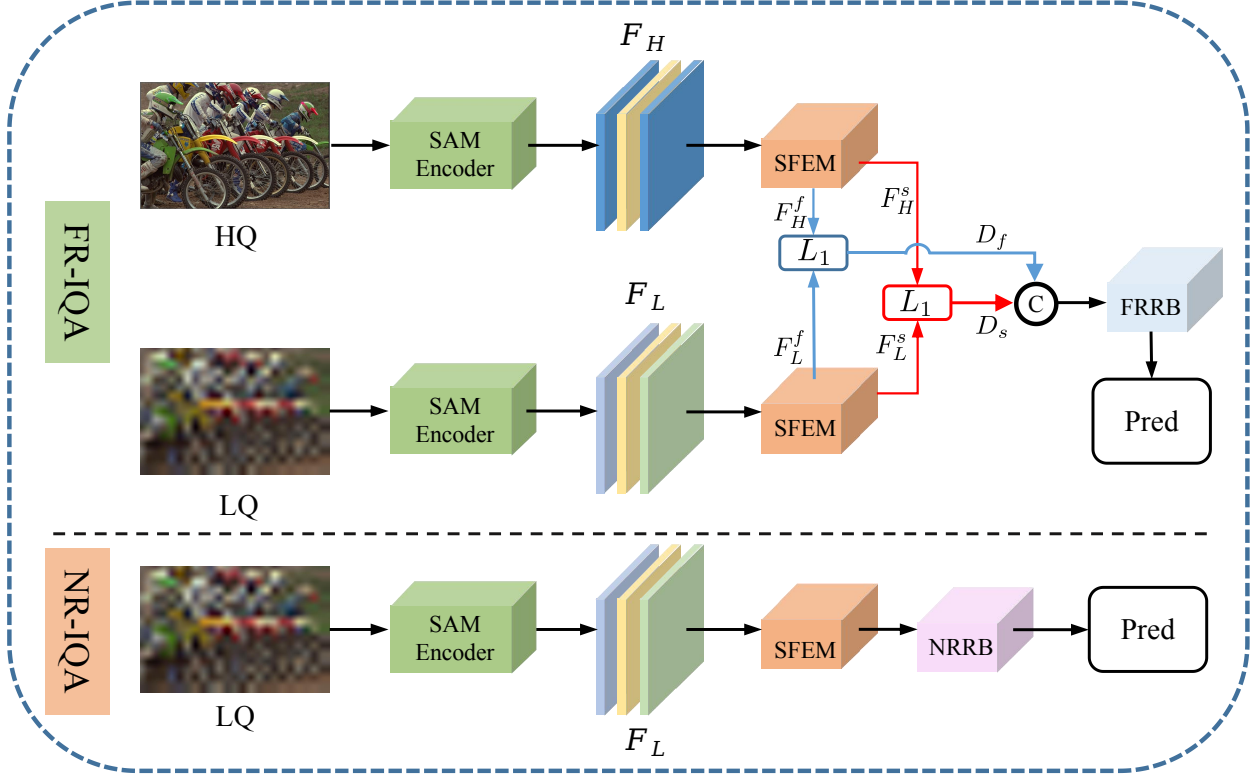


Figure 1. The pipeline of our method. The upper portion of this figure illustrates the FR-IQA process, while the lower portion describes the NR-IQA process. For FR-IQA, features are first extracted using SAM’s encoder, and then spatial-domain and frequency-domain features are extracted using a spatial-frequency feature extraction module (SFEM). Distances between HQ and LQ images are then measured separately in both domains, and these distances are fed into a regression block specifically designed for full-reference IQA (FRRB) to predict the final score. In contrast, for NR-IQA, only the LQ image is utilized as input, and features are extracted using SAM’s encoder. These features are further explored using SFEM, and a regression block designed for NR-IQA (NRRB) predicts the final score. Unlike FR-IQA, NR-IQA does not require any reference image for evaluation.

3. Method

3.1. Overall Architecture

As shown in Figure 1, our proposed approach enables both full-reference (FR) and no-reference (NR) image quality assessment. FR-IQA is a task that evaluates the quality of an image by comparing a degraded image with a corresponding reference image. Meanwhile, NR-IQA is a task that evaluates image quality without relying on any additional information beyond the input degraded image.

For full-reference IQA, we extract features F_L and F_H from the low-quality (LQ) and high-quality (HQ) images, respectively, using the encoder of SAM. Both F_L and F_H reside in a real space $\mathbb{R}^{256 \times 64 \times 64}$ and are fed into a spatial-frequency feature extraction module (SFEM), which is designed to extract spatial-domain and frequency-domain features and shares weights between them. The extracted features are then fed into a distance metric to obtain D_{LH} , which is used as input for a regression block (FRRB) specifically designed for full-reference IQA. FRRB predicts the

final score.

For no-reference IQA, we first extract features from the input degraded image using the encoder of SAM. We then extract spatial-domain and frequency-domain features using SFEM and feed them into a regression block (NRRB) specifically designed for no-reference IQA. Finally, NRRB predicts the final score.

3.2. Feature Extraction Using SAM

Previous work has utilized networks pre-trained on ImageNet to simulate the human experience in image evaluation. In this paper, instead of using a network pre-trained on ImageNet for feature extraction, we employ the encoder of a recently proposed segmentation model trained on massive amounts of data.

$$\begin{aligned} F_L &= \psi(I_{LQ}), \\ F_H &= \psi(I_{HQ}), \end{aligned} \quad (1)$$

where, I_{HR} denotes the input HQ image, I_{LQ} denotes the input LQ image, ψ represents the encoder of SAM, and F_L

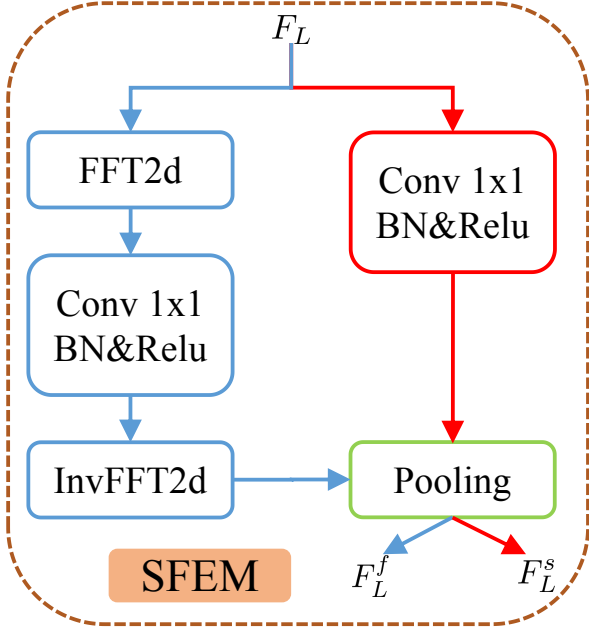


Figure 2. The structure of SFEM can be visualized in the following figure. In this architecture, features of different scales undergo similar operations. Specifically, two branches are employed: one utilizes Fourier convolution on the left to extract global features, while the other employs classical convolution to extract local features. To ensure compatibility across different feature sizes, an "AdaAvgPooling" method is employed for pooling, which converts results with varying sizes into a uniform size. This allows for effective fusion and enhancement of both local and global features within the SFEM framework.

and F_H denote the features obtained from I_{LQ} and I_{HQ} , respectively.

3.3. Spatial-Frequency Feature Extraction Module

After extracting semantic features using SAM, we utilize SFEM to further explore the features separately:

$$\begin{aligned} \{F_L^s, F_L^f\} &= \{\phi_s(F_L), \phi_f(F_L)\}, \\ \{F_H^s, F_H^f\} &= \{\phi_s(F_H), \phi_f(F_H)\}, \end{aligned} \quad (2)$$

where, ϕ_s represents the feature extraction network composed of regular convolutions, while ϕ_f represents the feature extraction network composed of Fourier convolutions. The symbol s denotes features belonging to the spatial domain, while f denotes features belonging to the frequency domain. The structure diagram is shown in Figure 2. According to the frequency-domain convolution theorem, convolutions at each point in the frequency domain can capture the global receptive field in the spatial domain. Therefore, utilizing both frequency-domain and spatial-domain convolutions can comprehensively explore image features by combining global and local feature representations.

3.4. Distance metric module

We use L_1 metric to measure the feature distance between the reference image and the distorted image in the spatial and frequency domains, respectively:

$$\begin{aligned} D_s &= L_1(F_L^s, F_H^s), \\ D_f &= L_1(F_L^f, F_H^f), \end{aligned} \quad (3)$$

where, D_s and D_f represent the feature distance between the reference image and the distorted image in the spatial and frequency domains, respectively. This step is used only for full-reference IQA.

3.5. Regression

Finally, we utilize the information obtained earlier to regress the quality score of the image, for full-reference IQA:

$$\tilde{y} = \Phi_f([f(D^s), g(D^f)]), \quad (4)$$

where f and g represent the mappings of spatial-domain and frequency-domain distances to the same distance space, respectively. Φ represents the regression network that maps the two types of distances to a quality score and $[*]$ represents the concatenation operation.

On the other hand, for NR-IQA:

$$\tilde{y} = \Phi_n([\eta_s(F_L^s), \eta_f(F_L^f)]), \quad (5)$$

where η_s and η_f represent the functions that map spatial-domain and frequency-domain features to the same feature space, respectively. The operation $[*]$ denotes concatenation, and Φ_n represents the regression network that predicts the score using the features.

After obtaining the predicted score, we utilize L_1 loss for supervised training:

$$loss = |\tilde{y} - y|. \quad (6)$$

4. Experiments

4.1. Experiment Settings

Datasets: This study employs four widely-used IQA datasets, namely LIVE [43], CSIQ [44], TID2013 [45] and KADID-10k [46], as shown in Table 2. LIVE and CSIQ are small-scale datasets, while TID2013 is medium-scale and KADID-10k is large-scale. The ground truth labels of TID2013 and KADIA-10k are represented by mean opinion score (MOS), while CSIQ and LIVE use differential mean opinion score (DMOS), which is inversely proportional to MOS. We adopt the common practice [19], [20] of randomly dividing each dataset into training, validation, and test sets with a ratio of 60%, 20%, and 20%, respectively.

Table 1. We conducted a comparison between our proposed method and other state-of-the-art approaches in two IQA tasks. The results are presented below, with the best performing results highlighted in bold and the second best results underlined. A dash ('-') indicates that the metric is not applicable.

IQA Type	Method	LIVE		CSIQ		TID2013		KADID-10k	
		SRCC	PLCC	SRCC	PLCC	SRCC	PLCC	SRCC	PLCC
FR-IQA	PSNR	0.873	0.865	0.810	0.819	0.687	0.677	0.676	0.675
	SSIM [18]	0.948	0.937	0.865	0.852	0.727	0.777	0.724	0.717
	VIF [30]	0.964	0.960	0.911	0.913	0.677	0.771	0.679	0.687
	PieAPP [31]	0.918	0.909	0.890	0.873	0.670	0.749	0.836	0.836
	LPIPS [32]	0.932	0.934	0.903	0.927	0.670	0.749	0.843	0.839
	DISTS [33]	0.955	0.955	0.946	0.946	0.830	0.855	0.887	0.886
	IQT [19]	0.970	-	0.943	-	0.899	-	<u>0.948</u>	<u>0.950</u>
	ISPL-FR [20]	<u>0.970</u>	<u>0.978</u>	<u>0.965</u>	<u>0.968</u>	0.924	0.912	0.944	0.943
	CVRKD [34]	0.960	0.965	0.958	0.965	<u>0.928</u>	<u>0.935</u>	0.957	0.959
	Ours	0.996	0.997	0.968	0.968	0.954	0.960	0.945	0.947
NR-IQA	BRISQUE [35]	0.939	0.935	0.746	0.829	0.604	0.694	-	-
	FRIQUEE [36]	0.940	0.944	0.835	0.874	0.680	0.753	-	-
	BMPRI [37]	0.931	0.933	0.909	0.934	0.928	0.947	-	-
	BIECON [38]	0.961	0.962	0.815	0.823	0.717	0.762	-	-
	WaDIQaM-NR [39]	0.954	0.963	-	-	0.761	0.787	-	-
	DIQaM-NR [39]	0.960	<u>0.972</u>	-	-	0.835	0.855	-	-
	IW-CNN [40]	<u>0.963</u>	0.964	0.812	0.791	0.800	0.802	-	-
	DB-CNN [41]	0.968	0.971	0.946	0.959	0.816	<u>0.865</u>	0.501	0.569
	HyperIQA [42]	0.962	0.966	<u>0.923</u>	<u>0.942</u>	<u>0.840</u>	0.858	0.852	0.845
	Ours	0.994	0.995	0.893	0.899	0.879	0.893	<u>0.815</u>	<u>0.814</u>

Table 2. Introduction to IQA datasets: The following table summarizes the characteristics of the IQA datasets used in this study. #Ref., #Dis., and #Dis.Type indicate the number of reference images, distorted images, and types of distortions, respectively.

Dataset	#Ref.	#Dis	#Dis.Type	Score Range
LIVE	29	779	5	[0,100]
CSIQ	30	866	6	[0,1]
TID2013	25	3000	24	[0,9]
KADID-10k	81	10125	25	[1,5]

Evaluation Criteria. We evaluate the performance of our proposed IQA method using two commonly used metrics: Spearman’s rank order correlation coefficient (SRCC) and Pearson’s linear correlation coefficient (PLCC), which have been widely employed in previous IQA approaches [19,20]. SRCC assesses the accuracy of the predicted rankings of image quality, while PLCC measures the correlation between the predicted scores and the ground truth scores.

4.2. Implementation Details

We utilized the ViT-H encoder, a large pre-trained model in SAM, to extract features for IQA. Our approach involved a two-stage process: first, we extracted features using the SAM encoder, and then we employed these saved features to train our subsequent IQA model. It’s important to note

that the SAM encoder was not fine-tuned during the training process.

To ensure effective training, we augmented the data by applying random horizontal and vertical flips to both the reference and distorted images. The training was conducted with a batch size of 16, using the ADAM optimizer with a learning rate of 2×10^{-5} . The model was trained for 500 epochs on NVIDIA-2080ti GPUs.

4.3. Comparisons with the State-of-the-art Methods

We conduct comprehensive evaluations of our proposed method against other state-of-the-art approaches in both FR-IQA and NR-IQA settings. In the FR-IQA experiments, we compare our method with widely used metrics such as PSNR, SSIM [18], and VIF [30], as well as recent methods including PieAPP [31], LPIPS [32], IQT [19], DISTS [33], ISPL [20], and CVRKD [34]. The results presented in Table 1 demonstrate the superior performance of our method across multiple datasets, including LIVE, CSIQ, TID2013, and KADID-10k. Our method consistently outperforms other approaches in all metrics, solidifying its effectiveness and promising capabilities in IQA.

In the NR-IQA experiments, we compare our method with representative and recent approaches including BRISQUE [35], FRIQUEE [36], BMPRI [37], BIECON [38], WaDIQaM-NR [39], DIQaM-NR [39], IW-CNN [40],

Table 3. We conducted a comparison between our proposed SAM encoder method and ResNet50 in the FR-IQA task. The results are shown below, with the best performing results highlighted in bold.

Method	LIVE		TID2013	
	SRCC	PLCC	SRCC	PLCC
ResNet50 [12]	0.979	0.982	0.949	0.958
Ours	0.996	0.997	0.954	0.960

Table 4. The SRCC is utilized to evaluate the performance of different branch forms in SFEM based on the FR-IQA type. In this context, we denote B represents the branch that uses classical convolution to extract local features and F represents the branch that uses Fourier convolution to extract global features.

B	F	LIVE	CSIQ	TID2013	LADID-10K
✓	✗	0.985	0.957	0.912	0.935
✗	✓	0.981	0.957	0.935	0.939
✓	✓	0.996	0.968	0.954	0.945

Table 5. Comparison of results using different methods to measure the distance between distorted and reference images in FR-IQA task. Among them, *sub.* indicates that the acquired features are directly subtracted, while *cos* and *KLD* mean Cosine similarity and Kullback-Leibler divergence.

Method	LIVE		CSIQ	
	SRCC	PLCC	SRCC	PLCC
<i>Sub.</i>	0.971	0.974	0.950	0.950
L_2	0.986	0.988	0.966	0.962
<i>cos</i>	0.990	0.991	0.967	0.966
<i>KLD</i>	0.987	0.989	0.965	0.965
L_1	0.996	0.997	0.968	0.968

DB-CNN [41], and HyperIQA [42]. The evaluation was conducted on datasets such as LIVE, CSIQ, TID2013, and KADID10k. Notably, our proposed method outperformed other methods across all metrics on the LIVE and TID2013 datasets. Additionally, it achieved promising results on the CSIQ and KADID10k datasets. These findings indicate the superior performance and versatility of our method in the realm of no-reference image quality assessment. The consistent superiority over other state-of-the-art approaches showcases the potential impact and applicability of our method in various real-world scenarios.

4.4. Ablation Study

The effectiveness of different encoders. We conduct comparative experiments on two encoders, including ResNet50 as our baseline and SAM’s encoder. The experimental results in Table 3 clearly demonstrate that utilizing the SAM’s encoder delivers the highest performance in the FR-IQA task. This finding solidifies the superiority of our pipeline constructed with the SAM’s encoder. Furthermore,

the comparative analysis highlights the enhanced capabilities provided by the SAM-based approach for image quality assessment.

The effectiveness of Fourier Convolution in SFEM. We conduct individual tests to evaluate the effectiveness of different branches within the SFEM framework in FR-IQA. Table 4 demonstrates that both classical convolution and Fourier convolution independently yield accurate predictions. However, when these two branches are combined, the local and global information complement each other, resulting in a further improvement in accuracy. This highlights the synergistic effect achieved by integrating both branches, allowing for more comprehensive and accurate assessments of image quality prediction.

The effectiveness of L_1 method as distance metric. We assess the effectiveness of different distance measurement methods for comparing distorted and reference images, as demonstrated in Table 5. We compared several commonly used methods, including L_2 , *cos*, and Kullback-Leibler divergence ((KLD)). The results indicate that the L_1 metric we utilized outperforms the other methods in the FR-IQA task. In scenarios involving reference frames, a simple L_1 metric is already effective enough to satisfy the requirements of our method, and it has consistently delivered satisfactory results in our experiments. These findings underscore the suitability and robustness of the L_1 metric for accurate image quality assessment.

5. Conclusion

In conclusion, our study presents a novel approach to Image Quality Assessment (IQA) that utilizes the Segment Anything (SAM) model for feature extraction. By leveraging the vast amount of training samples and strong generalization ability of SAM, we show that our method achieves state-of-the-art performance on various IQA datasets. We also draw attention to the importance of using frequency-domain features in IQA, which has been shown to better represent various distortions present in images. Our use of Fourier convolution in neural networks allows us to capture global features and relationships between image components, leading to improved accuracy in IQA. Overall, our work demonstrates the potential of incorporating advanced deep learning techniques into IQA and highlights the value of large-scale models trained on massive datasets for this task. To showcase the effectiveness of our method, we conducted extensive experiments covering diverse datasets and evaluation metrics, providing solid evidence of its superior performance in image quality assessment.

References

- [1] Youwei Li, Haibin Huang, Lanpeng Jia, Haoqiang Fan, and Shuaicheng Liu. D2c-sr: A divergence to convergence approach for real-world image super-resolution. In *Proc. ECCV*, pages 379–394, 2022. 1
- [2] Lei Yu, Xinpeng Li, Youwei Li, Ting Jiang, Qi Wu, Haoqiang Fan, and Shuaicheng Liu. Dipnet: Efficiency distillation and iterative pruning for image super-resolution. In *Proc. CVPR*, pages 1692–1701, 2023. 1
- [3] Ziwei Luo, Lei Yu, Xuan Mo, Youwei Li, Lanpeng Jia, Haoqiang Fan, Jian Sun, and Shuaicheng Liu. Ebsr: Feature enhanced burst super-resolution with deformable alignment. In *Proc. CVPR*, pages 471–478, 2021. 1
- [4] Ziwei Luo, Haibin Huang, Lei Yu, Youwei Li, Haoqiang Fan, and Shuaicheng Liu. Deep constrained least squares for blind image super-resolution. In *Proc. CVPR*, pages 17642–17652, 2022. 1, 2
- [5] Yawei Li, Yulun Zhang, Radu Timofte, Luc Van Gool, Lei Yu, Youwei Li, Xinpeng Li, Ting Jiang, Qi Wu, Mingyan Han, et al. Ntire 2023 challenge on efficient super-resolution: Methods and results. In *Proc. CVPR*, pages 1921–1959, 2023. 1
- [6] Jaakko Lehtinen, Jacob Munkberg, Jon Hasselgren, Samuli Laine, Tero Karras, Miika Aittala, and Timo Aila. Noise2noise: Learning image restoration without clean data. *arXiv preprint arXiv:1803.04189*, 2018. 1
- [7] Shen Cheng, Yuzhi Wang, Haibin Huang, Donghao Liu, Haoqiang Fan, and Shuaicheng Liu. Nbnnet: Noise basis learning for image denoising with subspace projection. In *Proc. CVPR*, pages 4896–4906, 2021. 1
- [8] Qi Wu, Mingyan Han, Ting Jiang, Haoqiang Fan, Bing Zeng, and Shuaicheng Liu. Realistic noise synthesis with diffusion models. *arXiv preprint arXiv:2305.14022*, 2023. 1
- [9] Zhen Liu, Wenjie Lin, Xinpeng Li, Qing Rao, Ting Jiang, Mingyan Han, Haoqiang Fan, Jian Sun, and Shuaicheng Liu. Adnet: Attention-guided deformable convolutional network for high dynamic range imaging. In *Proc. CVPR*, pages 463–470, 2021. 1, 2
- [10] Zhen Liu, Yinglong Wang, Bing Zeng, and Shuaicheng Liu. Ghost-free high dynamic range imaging with context-aware transformer. In *Proc. ECCV*, pages 344–360, 2022. 1
- [11] Eduardo Pérez-Pellitero, Sibi Catley-Chandar, Ales Leonardis, and Radu Timofte. Ntire 2021 challenge on high dynamic range imaging: Dataset, methods and results. In *Proc. CVPR*, pages 691–700, 2021. 1
- [12] Kaiming He, Xiangyu Zhang, Shaoqing Ren, and Jian Sun. Deep residual learning for image recognition. In *Proc. CVPR*, pages 770–778, 2016. 1, 6
- [13] Jacob Devlin, Ming-Wei Chang, Kenton Lee, and Kristina Toutanova. Bert: Pre-training of deep bidirectional transformers for language understanding. *arXiv preprint arXiv:1810.04805*, 2018. 1
- [14] Long Ouyang, Jeffrey Wu, Xu Jiang, Diogo Almeida, Carroll Wainwright, Pamela Mishkin, Chong Zhang, Sandhini Agarwal, Katarina Slama, Alex Ray, et al. Training language models to follow instructions with human feedback. *Proc. NeurIPS*, 35:27730–27744, 2022. 1
- [15] Tom Brown, Benjamin Mann, Nick Ryder, Melanie Subbiah, Jared D Kaplan, Prafulla Dhariwal, Arvind Neelakantan, Pranav Shyam, Girish Sastry, Amanda Askell, et al. Language models are few-shot learners. *Proc. NeurIPS*, 33:1877–1901, 2020. 1
- [16] Alexander Kirillov, Eric Mintun, Nikhila Ravi, Hanzi Mao, Chloe Rolland, Laura Gustafson, Tete Xiao, Spencer Whitehead, Alexander C Berg, Wan-Yen Lo, et al. Segment anything. *arXiv preprint arXiv:2304.02643*, 2023. 1
- [17] Lu Chi, Borui Jiang, and Yadong Mu. Fast fourier convolution. *Proc. NeurIPS*, 33:4479–4488, 2020. 2
- [18] Zhou Wang, Alan C Bovik, Hamid R Sheikh, and Eero P Simoncelli. Image quality assessment: from error visibility to structural similarity. *IEEE Trans. on Image Processing*, 13(4):600–612, 2004. 2, 5
- [19] Manri Cheon, Sung-Jun Yoon, Byungyeon Kang, and Junwoo Lee. Perceptual image quality assessment with transformers. In *Proc. CVPR*, pages 433–442, 2021. 2, 4, 5
- [20] Yue Cao, Zhaolin Wan, Dongwei Ren, Zifei Yan, and Wangmeng Zuo. Incorporating semi-supervised and positive-unlabeled learning for boosting full reference image quality assessment. In *Proc. CVPR*, pages 5851–5861, 2022. 2, 4, 5
- [21] Heliang Zheng, Huan Yang, Jianlong Fu, Zheng-Jun Zha, and Jiebo Luo. Learning conditional knowledge distillation for degraded-reference image quality assessment. In *Proc. CVPR*, pages 10242–10251, 2021. 2
- [22] Le Kang, Peng Ye, Yi Li, and David Doermann. Convolutional neural networks for no-reference image quality assessment. In *Proc. CVPR*, pages 1733–1740, 2014. 2
- [23] Da Pan, Ping Shi, Ming Hou, Zefeng Ying, Sizhe Fu, and Yuan Zhang. Blind predicting similar quality map for image quality assessment. In *Proc. CVPR*, pages 6373–6382, 2018. 2
- [24] Dingquan Li, Tingting Jiang, and Ming Jiang. Norm-in-norm loss with faster convergence and better performance for image quality assessment. In *Proceedings of the 28th ACM International Conference on Multimedia*, pages 789–797, 2020. 2
- [25] Hancheng Zhu, Leida Li, Jinjian Wu, Weisheng Dong, and Guangming Shi. Metaaiqa: Deep meta-learning for no-reference image quality assessment. In *Proc. CVPR*, pages 14143–14152, 2020. 2
- [26] Hamid R Sheikh, Muhammad F Sabir, and Alan C Bovik. A statistical evaluation of recent full reference image quality assessment algorithms. *IEEE Trans. on Image Processing*, 15(11):3440–3451, 2006. 2
- [27] Zhihe Lu, Zeyu Xiao, Jiawang Bai, Zhiwei Xiong, and Xinchao Wang. Can sam boost video super-resolution? *arXiv preprint arXiv:2305.06524*, 2023. 2

- [28] Jun Ma and Bo Wang. Segment anything in medical images. *arXiv preprint arXiv:2304.12306*, 2023. 2
- [29] Tao Yu, Runseng Feng, Ruoyu Feng, Jinming Liu, Xin Jin, Wenjun Zeng, and Zhibo Chen. Inpaint anything: Segment anything meets image inpainting. *arXiv preprint arXiv:2304.06790*, 2023. 2
- [30] Hamid R Sheikh and Alan C Bovik. Image information and visual quality. *IEEE Trans. on Image Processing*, 15(2):430–444, 2006. 5
- [31] Ekta Prashnani, Hong Cai, Yasamin Mostofi, and Pradeep Sen. Pieapp: Perceptual image-error assessment through pairwise preference. In *Proc. CVPR*, pages 1808–1817, 2018. 5
- [32] Richard Zhang, Phillip Isola, Alexei A Efros, Eli Shechtman, and Oliver Wang. The unreasonable effectiveness of deep features as a perceptual metric. In *Proc. CVPR*, pages 586–595, 2018. 5
- [33] Keyan Ding, Kede Ma, Shiqi Wang, and Eero P Simoncelli. Image quality assessment: Unifying structure and texture similarity. *IEEE Trans. on Pattern Analysis and Machine Intelligence*, 2020. 5
- [34] Guanghao Yin, Wei Wang, Zehuan Yuan, Chuchu Han, Wei Ji, Shouqian Sun, and Changhu Wang. Content-variant reference image quality assessment via knowledge distillation. *arXiv preprint arXiv:2202.13123*, 2022. 5
- [35] Anish Mittal, Rajiv Soundararajan, and Alan C Bovik. Making a “completely blind” image quality analyzer. *IEEE Signal processing letters*, 20(3):209–212, 2012. 5
- [36] Deepti Ghadiyaram and Alan C Bovik. Perceptual quality prediction on authentically distorted images using a bag of features approach. *Journal of vision*, 17(1):32–32, 2017. 5
- [37] Xionghuo Min, Guangtao Zhai, Ke Gu, Yutao Liu, and Xiaokang Yang. Blind image quality estimation via distortion aggravation. *IEEE Trans. on Broadcasting*, 64(2):508–517, 2018. 5
- [38] Jongyoo Kim and Sanghoon Lee. Fully deep blind image quality predictor. *IEEE Journal of selected topics in signal processing*, 11(1):206–220, 2016. 5
- [39] Sebastian Bosse, Dominique Maniry, Klaus-Robert Müller, Thomas Wiegand, and Wojciech Samek. Deep neural networks for no-reference and full-reference image quality assessment. *IEEE Trans. on Image Processing*, 27(1):206–219, 2017. 5
- [40] Jongyoo Kim, Hui Zeng, Deepti Ghadiyaram, Sanghoon Lee, Lei Zhang, and Alan C Bovik. Deep convolutional neural models for picture-quality prediction: Challenges and solutions to data-driven image quality assessment. *IEEE Signal processing magazine*, 34(6):130–141, 2017. 5
- [41] Weixia Zhang, Kede Ma, Jia Yan, Dexiang Deng, and Zhou Wang. Blind image quality assessment using a deep bilinear convolutional neural network. *IEEE Trans. on Circuits and Systems for Video Technology*, 30(1):36–47, 2018. 5, 6
- [42] Shaolin Su, Qingsen Yan, Yu Zhu, Cheng Zhang, Xin Ge, Jinqiu Sun, and Yanning Zhang. Blindly assess image quality in the wild guided by a self-adaptive hyper network. In *Proc. CVPR*, pages 3667–3676, 2020. 5, 6
- [43] Hamid R Sheikh. Image and video quality assessment research at live. <http://live.ece.utexas.edu/research/quality>, 2003. 4
- [44] Eric Cooper Larson and Damon Michael Chandler. Most apparent distortion: full-reference image quality assessment and the role of strategy. *Journal of electronic imaging*, 19(1):011006, 2010. 4
- [45] Nikolay Ponomarenko, Lina Jin, Oleg Ieremeiev, Vladimir Lukin, Karen Egiazarian, Jaakko Astola, Benoit Vozel, Kacem Chehdi, Marco Carli, Federica Battisti, et al. Image database tid2013: Peculiarities, results and perspectives. *Signal processing: Image communication*, 30:57–77, 2015. 4
- [46] Hanhe Lin, Vlad Hosu, and Dietmar Saupe. Kadid-10k: A large-scale artificially distorted iqa database. In *2019 Eleventh International Conference on Quality of Multimedia Experience (QoMEX)*, pages 1–3, 2019. 4